Two-phonon giant resonances in ^{136}Xe, ^{208}Pb, and ^{238}U

K. Boretzky,[1,2] A. Grünschloß,[1] S. Ilievski,[1,3] P. Adrich,[3,5] T. Aumann,[2,3] C. A. Bertulani,[3,*] J. Cub,[3,4] W. Dostal,[2] B. Eberlein,[2] Th. W. Elze,[1] H. Emling,[3] M. Fallot,[3] J. Holeczek,[3] R. Holzmann,[3] C. Kozhuharov,[3] J. V. Kratz,[2] R. Kulessa,[5] Y. Leifels,[3] A. Leistenschneider,[1] E. Lubkiewicz,[5] S. Mordechai,[6] T. Ohtsuki,[8] P. Reiter,[7] H. Simon,[4] K. Stelzer,[1] J. Stroth,[1] K. Sümmerer,[3] A. Surowiec,[3] E. Wajda,[5] and W. Walus[5]

(LAND Collaboration)

[1]*Institut für Kernphysik, Johann Wolfgang Goethe-Universität, D-60486 Frankfurt, Germany*
[2]*Institut für Kernchemie, Johannes Gutenberg-Universität, D-55099 Mainz, Germany*
[3]*Gesellschaft für Schwerionenforschung (GSI), Planckstrasse 1, D-64291 Darmstadt, Germany*
[4]*Institut für Kernphysik, Technische Universität, D-64289 Darmstadt, Germany*
[5]*Instytut Fizyki, Uniwersytet Jagielloński, PL-30-059 Kraków, Poland*
[6]*Ben-Gurion University of the Negev, Beer-Sheva, Israel*
[7]*Institut für Kernphysik, Universität Köln, D-50937 Köln, Germany*
[8]*Laboratory of Nuclear Science, Tohoku University, Sendai, Japan*

(Received 9 April 2003; published 28 August 2003)

The excitation of the double-phonon giant dipole resonance was observed in heavy projectile nuclei impinging on targets of high nuclear charge with energies of 500–700 MeV/nucleon. New experimental data are presented for ^{136}Xe and ^{238}U together with further analysis of earlier data on ^{208}Pb. Differential cross sections $d\sigma/dE^*$ and $d\sigma/d\theta$ for electromagnetic excitations were deduced. Depending on the isotope, cross sections appear to be enhanced in comparison to those expected from a purely harmonic nuclear dipole response. The cumulative effect of excitations of two-phonon states composed of one dipole and one quadrupole phonon, of predicted anharmonicities in the double-phonon dipole response, and of damping of the dipole resonance during the collision may account for the discrepancy. In addition, decay properties of two-phonon resonances were studied and compared to that of a statistical decay.

DOI: 10.1103/PhysRevC.68.024317 PACS number(s): 24.30.Cz, 25.70.De

I. INTRODUCTION

Giant resonances in atomic nuclei are collective resonant states at excitation energies above the nucleon separation energy, built by a coherent motion involving many nucleons. Such resonances can be viewed as a high-frequency but small-amplitude vibration that is damped by coupling to more complex states. In general, the damping width exceeds considerably the (γ, particle, fission) decay width and amounts to several MeV. In a quantal description, giant resonances are understood as the one-phonon state of a nuclear density or shape vibration. Since the vibration amplitude amounts to only a few percent of the relevant nuclear dimension, the vibration, to lowest order, should reflect harmonic properties. In reactions providing interaction times shorter than that of damping and decay, more than one phonon can be created forming the multiphonon giant resonances. Since they are embedded into a continuum of states with increasing density, selective probes and excitation mechanisms are required.

Double-phonon resonances were excited in pion double-charge-exchange reactions, selective to $|\Delta T_z|=2$ transitions [1]. Double excitation of the isoscalar giant quadrupole resonance was observed in heavy-ion reactions at intermediate energies [2]. Coulomb excitation in peripheral heavy-ion collisions at bombarding energies up to about 1 GeV/nucleon was found to populate the two-phonon isovector giant dipole resonance with rather large cross sections of several hundreds of millibarns [3]. From such measurements, the double-phonon excitation energies appear at about twice the single-phonon energies and their widths in between 1.5–2 times that of the single-phonon width, thus in line with a harmonic vibration picture. The respective experimental resolution, however, does not permit to conclude on small anharmonicities as expected on theoretical grounds (see below). In some cases, however, excitation cross sections seem to significantly deviate from those deduced from reaction models with an underlying ansatz of a harmonic giant resonance response.

The present paper comprises measurements aiming at the two-phonon giant dipole resonances (DGDR) in heavy nuclei. The DGDR peak energies in heavy nuclei are expected around 25–30 MeV excitation energy. Simple considerations show that the process of electromagnetic excitation in peripheral heavy-ion collisions at bombarding energies around 500–700 MeV/nucleon can reach out to such high excitation energies only via multistep excitations, almost exclusively of DGDR type. Thus, high-energy heavy-ion collisions provide a clean probe and were utilized in this study.

New experimental data are presented for the semimagic nucleus ^{136}Xe and the quadrupole-deformed and fissile nucleus ^{238}U, together with a further analysis of data from an earlier experiment on the doubly magic nucleus ^{208}Pb. In case of ^{136}Xe, the present experiment manifests a remeasurement of earlier data obtained by the same collaboration [4],

*Present address: NSCL, East Lansing, Michigan 48824, USA.

now performed with an improved experimental technique.

II. THE EXPERIMENTS ON ^{136}Xe, ^{208}Pb, AND ^{238}U

Within this paper, we present results from three separate experiments performed at the heavy-ion synchrotron (SIS) facility at GSI, Darmstadt. These studies were devoted to an investigation of the double-phonon giant dipole resonance employing electromagnetic excitation of the projectiles ^{136}Xe, ^{208}Pb, and ^{238}U at high bombarding energies (500–700 MeV/nucleon) on heavy targets of high nuclear charge. In heavy nuclei as investigated here, the decay of giant resonances is dominated by neutron evaporation and subsequent γ decay of the residual fragment. In case of ^{238}U, the fission decay channel competes with neutron emission.

The experimental apparatus allowed for a semiexclusive measurement including the fragment and emitted neutrons and γ rays, from which the primary excitation energy of the projectiles was reconstructed and, therefore, energy-differential cross sections are accessible. In addition, neutron and γ-decay spectra were analyzed. In case of ^{136}Xe, the angular distribution of the scattered projectile was also measured.

The semimagic nucleus ^{136}Xe was the first nucleus for which such a kinematical experiment was carried out [4]. It yielded a considerable cross section enhancement for the DGDR. The data on ^{136}Xe presented here, stem from a measurement with an improved setup. Improvements concerned especially the fragment mass measurement, the γ-detection system, and the determination of the fragment scattering angle. The latter is important for the angular differential cross section measurement which was already published in Ref. [5]. Here, the ^{136}Xe results will be supplemented with the energy-differential cross sections from three different targets.

The findings of the experiment performed on the doubly magic nucleus ^{208}Pb were partly published in Ref. [6]. In this paper, we deliver additional information about the excitation spectra measured with five different targets (U, 2×Pb, Ho, Sn) and discuss the decay characteristics, leading to an experimental value for the spreading width of the DGDR.

For the deformed and fissile nucleus ^{238}U, inclusive data on the DGDR exist for the neutron decay [7] and for the fission decay [8–10], which led to inconsistent conclusions concerning a possible enhancement of the DGDR strength. The DGDR cross section obtained from the neutron decay was found to be consistent with that expected from the harmonic approximation, the data from the fission decay indicated a cross section enhancement. From the present experiment of more exclusive type, the energy differential cross sections for the neutron decay of ^{238}U after Coulomb excitation on Pb and Sn targets at 500 MeV/nucleon were obtained. The fission decay channel, also covered in this measurement, is currently analyzed and will be published in a forthcoming communication.

III. THE EXPERIMENTAL METHOD

As the experimental method and setup for the three measurements are similar, we discuss it in detail only for the ^{136}Xe case (Sec. III A). Modifications in case of the other two experiments, as far as being substantial, are described in Secs. III B and III C.

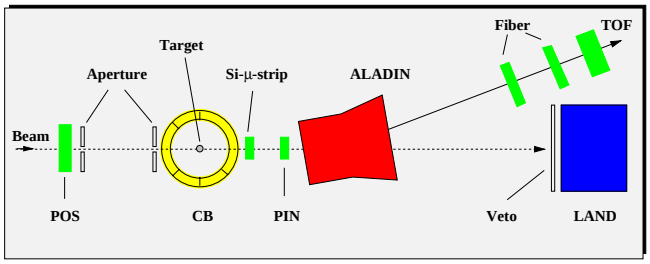

FIG. 1. (Color online) Schematic view of the experimental setup. Shown are the beam and fragment counters (see text), the dipole magnet (ALADIN), the 4π NaI Crystal Ball γ spectrometer (CB), and the neutron detector (LAND).

A. The ^{136}Xe experiment

1. Techniques and observables

As already mentioned, we employ the method of projectile excitation on a heavy target, which leads to large excitation cross sections due to the Coulomb interaction between projectile and target. At high bombarding energies, here 500–700 MeV/nucleon, dipole excitations of high-lying collective states occur with cross sections of the order of barns for the GDR, and of the order of several hundreds of millibarns for the DGDR [3].

In our approach, the excitation energy E^* of the projectile is reconstructed by a kinematical complete measurement covering all products of the decaying system.

The experimental setup for the ^{136}Xe experiment is shown schematically in Fig. 1. It consists of a number of detectors measuring time of flight, position, and energy loss of both the incoming projectile and outgoing projectile fragment, thus enabling the determination of momentum, charge, mass, and the scattering angle of the heavy fragment. The neutrons emitted from the excited projectile are detected in the large area neutron detector (LAND), their momenta are determined from position and time-of-flight information. Energies and angles of the emitted γ rays are measured with the 4π NaI spectrometer Crystal Ball (CB). This information allows for an event-by-event reconstruction of the excitation energy E* by analyzing the invariant mass M through

$$M^2 = \left(\sum_i P_i \right)^2 = (M_P + E^*)^2, \tag{1}$$

where P_i denote the four-momenta of all dissociation products and M_P the projectile rest mass. In this way, the energy-differential cross section distributions are obtained. Likewise, from the spatial components of the four-momenta, momentum or angular distributions can be deduced. Kinetic energy spectra of emitted neutrons or γ-ray spectra, for instance, can also be transformed into the projectile center-of-mass frame. The experimental setup is explained in detail in the following section.

2. Detection system

The $^{136}_{54}$Xe projectiles in an atomic charge state 46^+ were accelerated by the SIS to 700 MeV/nucleon. After extraction, the beam passed a diaphragm with a 1 mm circular aperture. Only ions passing the aperture were transported by the beam line to the experimental area, while particles hitting the diaphragm material became essentially fully stripped and were removed from the beam by deflecting magnets. This method allowed for an efficient reduction of the beam emittance, which is of substantial importance in order to perform the scattering angle measurement.

The Xe projectiles hit a position sensitive organic scintillator detector (POS), which acts also as start counter for the time-of-flight measurement. The detector with an active area of 5×5 cm^2 and a thickness of 25 mg/cm^2 was located about 10 m upstream from the target. The scintillator was coupled to four phototubes allowing, from their relative light output, to determine the position of incidence in both directions (x,y) perpendicular to the beam with a resolution of $\sigma_{x,y}=0.5$ mm. In order to avoid angular straggling effects in front of the target, instead of a second position sensitive detector, an active four-jaw beam collimator was placed 1.5 m in front of the target. Projectiles hitting the collimator were rejected by the trigger decision. The aperture is chosen to be 1 mm$\times$1 mm (3 mm$\times$3 mm) for a thin Pb target (for other targets). An additional active four-jaw beam collimator with an aperture of 10 mm$\times$8 mm placed directly behind POS served to control the beam size. In a distance of 1 m behind the target, two single-sided Si-strip detectors of 100 μm pitch and 150 μm thickness were used to measure the (x,y) position of the scattered fragments after the reaction in the target. From the measured trajectories of both the incoming and outgoing Xe ions the scattering angle Θ can be deduced which, for Coulomb scattering at energies as high as in this experiment, amounts to values below $\Theta_{max.}\approx8$ mrad, see Sec. IV A. Two p-i-n silicon diodes (PIN) with a thickness of 170 μm were placed behind the target in order to obtain the charge of the fragments with a resolution of about 1% (full width at half maximum, FWHM).

The charged fragments were deflected by a dipole magnet (ALADIN) with a large gap, and their trajectories were further determined in the dispersive plane from the one-dimensional position information of two scintillating fiber detectors with a pitch of 1 mm [11]. The position measurements determine the magnetic rigidity of the fragments. Time-of-flight information and a second charge identification was obtained from a detector array (TOF) of thin organic plastic scintillators of 2 m$\times$2 m size and placed about 7 m behind the magnet. Integrating the information on nuclear charge, magnetic rigidity, and time of flight, the fragment mass can be analyzed. The mass resolution depends on the target thickness, for the measurement with the thin Pb target a resolution equivalent to $\Delta A/A=0.0058$ (FWHM) was achieved. The target position was surrounded by a 4π array of 162 NaI modules for the detection of the γ rays emitted after projectile excitation, the (CB) spectrometer.

The neutrons evaporated from the excited projectile are detected about 11 m downstream from the target in the LAND [12], centered around the beam direction. Due to the kinematical forward focusing of neutrons emitted from the high-energy projectile, essentially the full neutron solid angle is covered. The LAND detector with a size of 2 m$\times$2 m and 1 m depth is built from 200 modules, each one of a volume of 0.1 m$\times$2.0 m$\times$0.1 m and consisting of alternating layers of scintillator and iron material. Each module is read out from the two far sides by photomultipliers, delivering timing information. From the sum of the two time signals, the neutron time of flight, and from the time difference, the neutron position of incidence can be derived. An array of organic plastic scintillators (Veto) in front of LAND served to reject incident charged particles. The LAND detector is calibrated using the recognition of tracks from cosmic rays traversing the detector and inducing signals in several modules. The time resolution of the modules amounts to about $\Delta t=500$–600 ps (FWHM) and the position resolution to $\Delta x=7$–10 cm. The absolute time-of-flight calibration between target and the LAND detector was achieved by utilizing high-energy γ rays emitted in more central nuclear collisions between projectile and target. Multineutron hits are analyzed from their hit pattern provided by the modular detector structure. The detection capabilities of LAND were studied in detail in a calibration experiment using tagged neutrons from the breakup of a deuteron beam at various beam energies. The one-neutron detection efficiency is shown in Fig. 2 as a function of the neutron energy in the laboratory frame. In case of the Xe experiment it results in $\varepsilon_{1n}=0.95$.

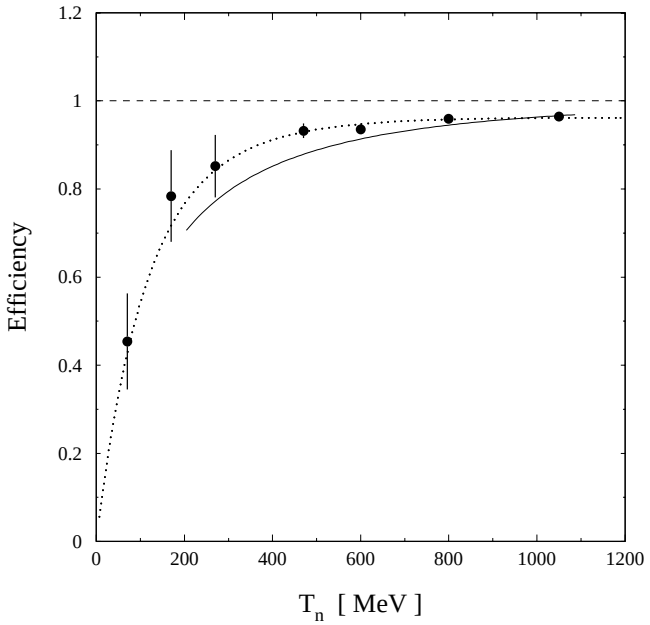

FIG. 2. LAND detection efficiency for neutrons of energy T_n. The dotted line presents a fit to the data of the calibration experiment, the solid line shows the predictions of a detector simulation. The simulation underestimates the measured efficiency towards lower neutron energies because secondary particles were traced down to 50 MeV kinetic energy only.

For neutrons emitted with kinetic energies of $T_{kin}=0.5$, 1, and 4 MeV in the projectile center-of-mass frame, a resolution of $\sigma(T_{kin})=0.36$, 0.45, 1.0 MeV was obtained, respec-

tively. The multineutron recognition was studied applying an event-mixing technique using the deuteron breakup data. For the case of DGDR studies, an event misinterpretation towards a too high neutron multiplicity would lead to severe changes in the shape of the energy-differential cross section due to the additional binding energy assigned to this artificial neutron. The procedure for the identification of multineutron hits, therefore, was optimized such that the misinterpretation towards a too high neutron number was nearly completely suppressed. Under these conditions, the efficiencies to detect the correct neutron multiplicity reduce to 0.71, 0.38, and 0.16 for neutron multiplicities of 1, 2, and 3, respectively. The misidentification is substantially reduced by requiring that the neutron decay multiplicity matches with the observed Xe fragment mass within resolution. This requirement not only reduces a misidentification of the neutron multiplicity, it also eliminates, to a large extent, nucleon knockout reactions, since in knockout reactions, neutrons are scattered to large angles beyond the acceptance of LAND.

The ^{136}Xe beam is directed onto different targets, i.e., ^{208}Pb (1060 mg/cm^2), ^{208}Pb (54 mg/cm^2), ^{nat}Sn (239 mg/cm^2), and ^{nat}C (274 mg/cm^2) targets. The carbon target served to control cross section contributions originating from nuclear interactions. An additional measurement was performed without inserting a target in order to determine background contributions from beam ions interacting in detector or other materials (the flight path of the heavy ions was kept under vacuum up to the TOF detector).

During the whole experiment, events without interaction of the primary beam were registered in a downscaled mode allowing to normalize properly the measured cross sections.

3. Detector response and experimental filter

As stated above, in heavy nuclei such as Xe or Pb, giant resonances decay essentially by neutron evaporation. In consequence, reaction channels were selected and analyzed for which the nuclear charge of the projectile was preserved but yielded the emission of up to three neutrons. Higher neutron decay multiplicities did not contribute significantly.

In a first step, the geometrical acceptance of our detector system for these reaction channels was examined empirically. From the position distribution of neutrons in LAND, a geometrical acceptance of 97% for single neutrons was determined. For the projectile fragment, the solid angle coverage depends on the mass of the fragment since the deflection in the dipole magnet depends on the fragment magnetic rigidity. For the same reason, the acceptance also depends slightly on the target (thickness). For example, for the thick Pb-target a geometrical acceptance for the projectile fragment of 80%, 74%, and 63% for the $1n,2n,3n$ removal channels was determined, respectively.

The detection response with respect to excitation energy is determined by two major components, the neutron recognition, especially for multineutron events in LAND, and the response of the γ-ray spectrometer.

As far as the γ-ray detection is concerned, the experimental resolution severely suffers from atomic interactions. Atomic interactions of the beam with the heavy targets induce a large x-ray and bremsstrahlung background which depends on the nuclear charge of target and projectile as well as on beam energy (see Ref. [13] and references therein). This background could be determined in our experiment by analyzing the γ-ray spectra for projectiles which did not undergo nuclear interactions. For example, the average energy deposit in the Crystal Ball spectrometer due to atomic interactions was found to amount to 6.5 MeV with a standard deviation of 2.1 MeV in case of the thick lead target, which represents the worst case; an average energy deposit of only 0.9 MeV was observed for the tin target.

This average energy deposit can be subtracted on an event-by-event basis, but the inherent statistical distribution leads to a considerable smearing of the γ-ray detection response. In order to reduce this effect, we decided to utilize only the forward hemisphere of the Crystal Ball spectrometer. Since the atomic background exhibits a nearly isotropic angular distribution, it is reduced by a factor of 2, while the efficiency to detect γ rays from the projectile is reduced by only 20% due to the Lorentz boost.

The response behavior of the detection system is well understood but, nevertheless, too complex to be deconvoluted from the measured spectra in a straightforward manner. In consequence, instead of attempting a deconvolution of the spectra, we decided to construct an ''experimental filter'' that needs to be applied to theoretically obtained cross section distributions prior to comparison with the experimental results. This filter simulates in a Monte Carlo technique the response of the various components of the detection system, but also physical effects as those of the atomic background discussed above.

In this procedure, the decay has to be modeled for a given calculated differential excitation cross section. For each adopted excitation energy, first, the decay channel is chosen according to $\Gamma_{xn}/\Gamma_{tot}(E^*)$ data from photoabsorption measurements (for details see Ref. [4] and references cited therein). The neutron and subsequent γ-ray decays are then described according to the statistical model, which is steered by level density parameters within the continuum and by known low-lying bound states. Provisions are taken to describe also nonstatistical direct decay components, as observed, e.g., for the ^{208}Pb case in Ref. [14]. In a second step, the detector response is incorporated.

(i) The resolutions for the Xe fragment detectors were implemented.

(ii) The neutron detector response was taken from the deuteron breakup calibration measurement. Therein, events of higher neutron multiplicity were produced from the deuteron calibration applying an event mixing technique.

(iii) The response with regard to γ-ray observation was deduced from detailed GEANT simulations which were checked by means of calibration data using standard γ-ray sources. The experimentally determined atomic background was added on top of it, see above. Finally, the simulated data were analyzed in the same manner as the experimental data applying identical selection criteria, and were only then compared to each other.

Figure 3 shows an example of the modification of the input cross section distribution due to the experimental filter for one-phonon giant dipole and quadrupole resonances in

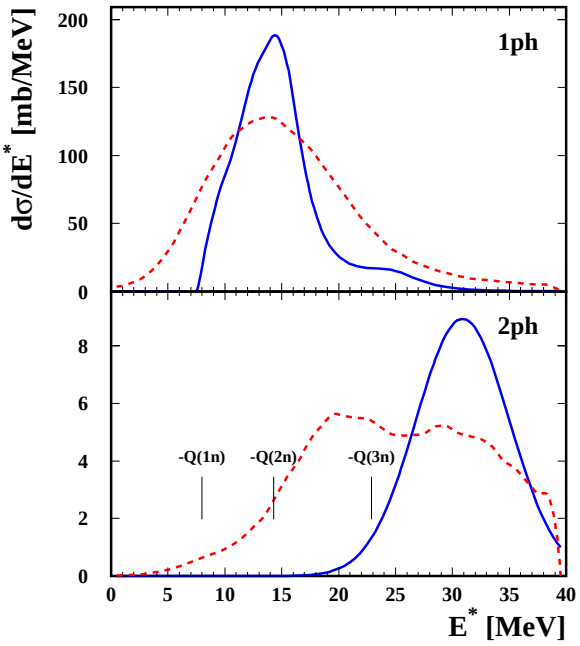

FIG. 3. (Color online) Upper panel: The solid line shows the energy-differential electromagnetic cross section of one-phonon giant dipole and quadrupole resonances excited in ^{136}Xe projectiles (700 MeV/nucleon) impinging on a thick Pb target as calculated within the semiclassical approach using resonance parameters from literature (see Table I). The dashed line represents the modification of this distribution due to the experimental filter. Lower panel: Same as upper panel, however for the double-phonon giant dipole resonance as obtained from the folding model. Thresholds $(-Q)$ for the decay into one, two, and three neutrons are indicated.

the upper part and for the double-phonon giant dipole resonance in the lower part for the case of ^{136}Xe impinging on the thick Pb target.

As seen for the example for the one-phonon resonance, the calculated curve is smeared out due to the experimental resolutions. The major part of this effect is explained by the large amount of atomic background in the γ-ray measurement using the thick Pb target. For the DGDR, we observe that part of the cross section is shifted towards lower excitation energies, essentially due to a misinterpretation of the number of emitted neutrons.

The input to the theoretical cross section distributions and to the filter determining the decay mode will be discussed in detail in Sec. IV.

B. The ^{208}Pb experiment

The setup used for ^{208}Pb projectiles (640 MeV/nucleon) is described in Ref. [6]. The main differences compared to the Xe experiment concern the γ detector, which consisted of 66 BaF_2 crystals surrounding the target, leading to a reduced efficiency.

A rather systematic measurement was performed using six different targets, i.e., U (238 mg/cm^2), Pb (256 and 798 mg/cm^2), Ho (800 mg/cm^2), Sn (500 mg/cm^2), and C (180 mg/cm^2), all of natural abundance. The intention was to distinguish between one- and two-step excitations and to disentangle electromagnetic and nuclear contributions, see Sec. V.

C. The ^{238}U experiment

The nucleus ^{238}U has a fission threshold around 5 MeV excitation energy, and thus giant resonances may decay by neutron emission as well as by fission. The fission probability increases with excitation energy, therefore higher-phonon states should be ''enhanced'' in the fission channel. The major difference in the setup of the U experiment compared to the Xe experiment resulted from the request of detecting both fission fragments in addition to the neutron decay channel. Therefore the fragment counters had to be subdivided into two active arrays placed on both sides of the beam trajectory. This is of influence also for the neutron decay measurement, because the inactive area between the two arrays led to a certain reduction in projectile fragment acceptance. Here, we report only results from the neutron decay channel, details of the fission measurement will be reported in a forthcoming publication. Furthermore, instead of the full CB array for the γ-ray detection only part of the NaI crystals were available. A total of 33 crystals were mounted in forward direction, and 41 crystals formed a ring surrounding the target at 90°.

The experiment utilized an ^{238}U beam at an energy of 500 MeV/nucleon impinging on natural Pb (302 mg/cm^2), Sn (239 mg/cm^2), and C (274 mg/cm^2) targets.

IV. DATA ANALYSIS AND RESULTS FOR ^{136}Xe

A. Angular differential cross section data

As will be discussed later, the analysis of our data relies heavily on a description of electromagnetic excitation processes within the semiclassical approximation. Classical trajectories are characterized by the impact parameter b. Nuclear processes are taken into account as an (partial) absorption of the incoming flux for collisions at small internuclear distances within the reach of the nuclear force. The key parameter is the minimum impact parameter around which nuclear absorption starts to dominate. This minimum impact parameter needs to be determined empirically. One aim of the Xe experiment was thus to measure angular fragment distributions after Coulomb excitation. At high energies (here 700 MeV/nucleon), Coulomb scattering leads to small scattering angles Θ of the fragment in the laboratory system, which are connected to the impact parameter b of the reaction by

$$\Theta = \frac{2Z_p Z_t e^2}{b v^2 \gamma m_p}, \tag{2}$$

where Z_p and Z_t represent the nuclear charge of the collision partners, m_p the rest mass and v the velocity of the projectile, and γ the Lorentz factor. The experimental challenge of a precise angular measurement with maximum scattering angles below 10 mrad requires a setup with a minimum of detector material passed by the ions and thin targets in order to reduce angular straggling, and very precise position mea-

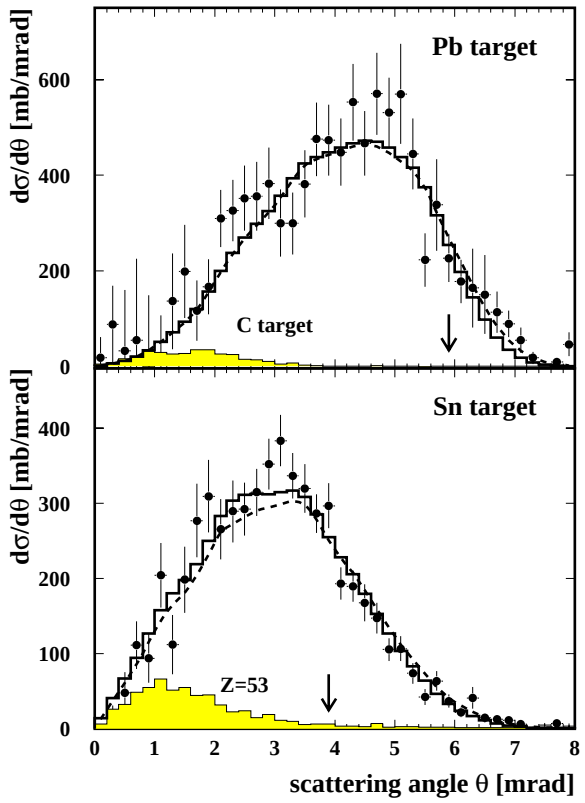

FIG. 4. (Color online) Angular differential cross section for the Coulomb excitation of ^{136}Xe (700 MeV/nucleon) on a Pb target (upper panel) and on a Sn target (lower panel). The data are compared with semiclassical calculations using a sharp cutoff minimum impact parameter b_{min} (solid lines) and a smooth cutoff from the soft-spheres model (dashed lines). Arrows indicate scattering angles corresponding to b_{min}. The calculated distributions are convoluted with the experimental resolution. The shaded areas show the amount of nuclear contributions determined from the measurement with the C target (upper panel), and for a one-proton removal reaction in the Sn target (lower panel).

surements. Here, we used ^{208}Pb (54 mg/cm^2), ^{nat}Sn (239 mg/cm^2), and ^{nat}C (274 mg/cm^2) targets. The overall angular resolution (including small-angle straggling) of our detector setup as described above resulted in a width of $\sigma_\Theta = 0.62$ (1.20) mrad for the Pb (Sn) target. Details of this part of the experiment are found in Ref. [5], here we summarize results only to the extent needed for further discussion.

The differential cross sections $d\sigma/d\Theta$ are presented in Fig. 4 for the measurement on the Pb and Sn targets. The spectra are dominated by electromagnetic excitation. In order to judge on the amount of nuclear excitations we contrast the cross section distributions with the spectrum obtained for the carbon target (upper panel of Fig. 4), and with a spectrum for the Sn target but requiring a fragment charge of $Z=53$ (lower panel of Fig. 4), both of which are essentially determined by nuclear interactions. In the latter case, one could argue that electromagnetic excitations may also contribute to the one-proton removal reaction. Statistical emission of protons from excited heavy nuclei, however, is strongly suppressed by the Coulomb barrier. A nonstatistical neutron decay component is observed in the data as outlined in the following section with an upper limit of about 20 mb in case of the Sn target. A corresponding proton-decay component may contribute to the proton-removal channel, but obviously, the proton decay from the giant resonance domain is much smaller than the neutron decay. The procedure of subtracting the contribution to the neutron decay channels arising from nuclear excitations is described in the following section.

TABLE I. Resonance parameters for the GDR and the GQR$_{is,iv}$ in ^{136}Xe as adopted from literature. The strength is quoted as a percentage of the related energy-weighted sum rules.

	E_{1ph} (MeV)	Γ (MeV)	Strength (%)
GDR	15.3	4.9	110–140
GQR$_{is}$	12.6	3.3	80–120
GQR$_{iv}$	25.3	6.5	80–120

For the interpretation of the spectra, the impact parameter dependent Coulomb excitation cross section is computed in a semiclassical approach [15]. Excitations of the isovector giant dipole resonance (GDR), the isoscalar and isovector giant quadrupole resonances (GQR$_{is,iv}$), and the DGDR are taken into account. According to the fact that xenon is gaseous, no experimental data on the giant resonance parameters exist. Therefore, the parameters of the GDR as well as the photoneutron decay channels needed to be interpolated from photoabsorption measurements of the neighboring nuclei, i.e., ^{133}Cs and ^{138}Ba [16], which leads to an uncertainty of about 15% in the integrated strength. The parameters for the GQR$_{is,iv}$ are extracted from the data systematics given in Refs. [17,18] and [19], respectively, the integrated strength exhibiting an uncertainty of about $\pm 20\%$. The adopted giant resonance parameters are given in Table I.

The contribution from the DGDR was obtained within the folding model [20], see also below. The excitation of the single GDR delivers by far the strongest contribution to the cross sections. The most crucial point in these calculations concerns the treatment of impact parameters within the region of grazing incidence, where the nuclear absorption sets in. In literature, frequently a ''sharp-cutoff'' approximation is applied, with a ''minimum impact parameter'' b_{min} separating the domains of Coulomb and nuclear interactions. Different parametrizations for the choice of this value b_{min} exist [21,22]. Alternatively a ''smooth cutoff'' may be used, as proposed in Ref. [23] with the ''soft-spheres'' model. The angular distributions calculated in semiclassical approximation for various choices of b_{min} were convoluted with the instrumental resolution and then compared to the data. Figure 4 shows the best fit for a sharp-cutoff minimum impact parameter b_{min} resulting from a χ^2 analysis (solid line) and the distribution obtained from the soft-spheres model (dashed line). The experimental angular resolution, unfortunately, masks the differences in the distributions predicted by the two models. In case of the sharp-cutoff approximation, values of $b_{min}^{expt} = 14.5 \pm 0.4$ fm and $b_{min}^{expt} = 13.6 \pm 0.6$ fm are obtained from the fits for the Pb and Sn targets, respectively. For the Pb target b_{min}^{expt} is in perfect agreement with the parametrization of Benesh, Cook, and Vary (BCV) [21], the parametrization of Kox [22] gives a too large value. For the

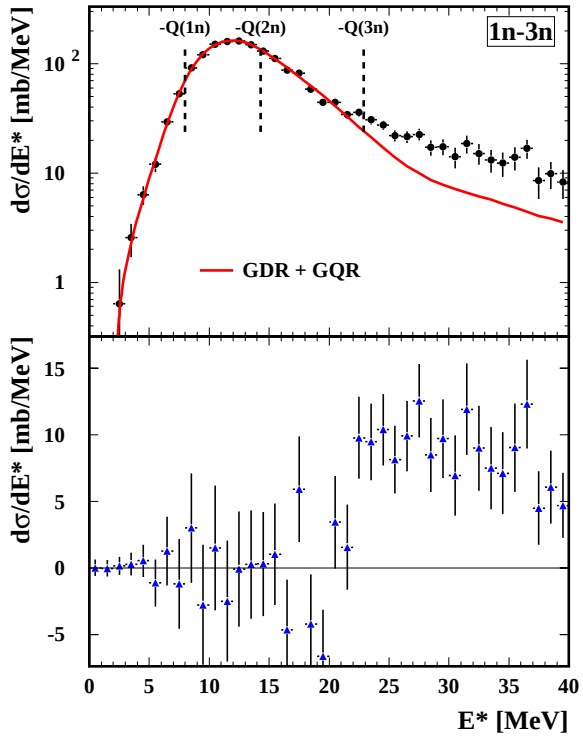

FIG. 5. (Color online) Upper panel: Experimental differential cross section $d\sigma/dE^*$ for ^{136}Xe and the thick Pb target. Threshold energies $(-Q)$ for the separation of one to three neutrons are indicated. The solid line represents the calculated sum of cross sections for one-phonon giant dipole and quadrupole resonances. Lower panel: Difference in measured and calculated cross sections from upper panel.

Sn target, b_{min}^{expt} is found in between that of the BCV and that of the Kox parametrization. In any case, the measurement of the angular cross section distributions shows that the spectra can be well described within the semiclassical approximation with a proper choice of b_{min}. A more detailed discussion of these data is given in Ref. [5].

B. The excitation energy spectra

From the invariant mass, Eq. (1), of the Xe fragment and the emitted neutrons and γ-rays, the ^{136}Xe excitation energy E^* is obtained event-by-event and the energy differential cross sections $d\sigma/dE^*$ can be deduced. The spectrum for the thick Pb target is shown in Fig. 5. The background measured without target, contributing 15% to the cross section, is already subtracted. By using the measurement with the C target, moreover, the nuclear cross section was estimated and was also subtracted. For that purpose, the measurement on the C target was analyzed under identical conditions as for the Pb target. For the C target, electromagnetic excitations can be neglected and the observed cross sections can be assigned solely to nuclear excitations. Cross sections of nuclear neutron-removal reactions in heavy-ion collisions can be scaled with the radii of the interacting nuclei as discussed in Ref. [24]. From a fit on the systematics of experimental data using the ''factorization model'' [25–27], a scaling can be derived of the form

$$\sigma_{Tar}^{nucl.} = \frac{1 + aA_{Tar}^{1/3}}{1 + aA_{C}^{1/3}} \sigma_C \tag{3}$$

with $a = 0.14(0.01)$ as shown in Ref. [28]. The nuclear contributions determined according to the above scaling prescription amount to 5% for the Pb targets and 10% for the Sn target, thus are small in both cases. It should be noticed that the experimental cross section distribution as shown in Fig. 5 extends to excitation energies below the one-neutron separation threshold. This effect arises, because only the mean γ-energy deposit of the atomic background distribution can be subtracted.

In order to analyze the measured differential cross sections $d\sigma/dE^*$ and eventually to extract the double-phonon components, we proceed in the following manner:

(i) The distributions of the single-phonon dipole and quadrupole strength over excitation energy were adopted from independent measurements, see Table I and above.

(ii) From these distributions, the electromagnetic excitation cross sections for the heavy-ion collisions of interest were computed in semiclassical approximation, and a sharp cutoff minimum impact parameter according to the BCV parametrization was chosen as it was found to be consistent with the analysis of the angular distributions discussed in the preceding section. Multistep excitations depleting to some extent the excitation of single giant resonance phonons in favor of higher-phonon states were taken into account by applying the ''folding model'' [20]. The folding model describes correctly the electromagnetic multistep excitations within the equidistantly spaced levels of a harmonic oscillator and also accounts for the nonzero width of the giant resonances. Throughout this paper, cross sections computed within the folding model serve as reference for a harmonic response with regard to multiphonon states, as frequently used in literature.

(iii) The calculated cross sections are passed through the experimental filter and are then compared to the experimental data. For the experimental filter, modeling of the decay of the excited nuclei is required as was outlined in Sec. II A 2. For ^{136}Xe, level density parameters were taken from Refs. [29,30].

In a first approach of data analysis, cross sections calculated in this manner for the sum of single-phonon giant dipole and quadrupole resonance excitations are compared to the measurement in Fig. 5. The only free parameter in the calculation was that of the overall normalization being adjusted at lower excitation energies. Below an excitation energy of 20 MeV, we observe a perfect description of the experimental data. Above 20 MeV, an excess in experimental cross section is found, centered around 30 MeV.

For the final analysis, we parametrize the excess cross section by a Gaussian distribution. In a χ-square fitting procedure applied simultaneously to all spectra obtained for the three different targets, the centroid and width of the Gaussian distribution were determined, the normalization of both the single-phonon cross sections and that of the excess cross section were adjusted individually for each target. In this way, we obtain excess cross sections of 163(20) mb and

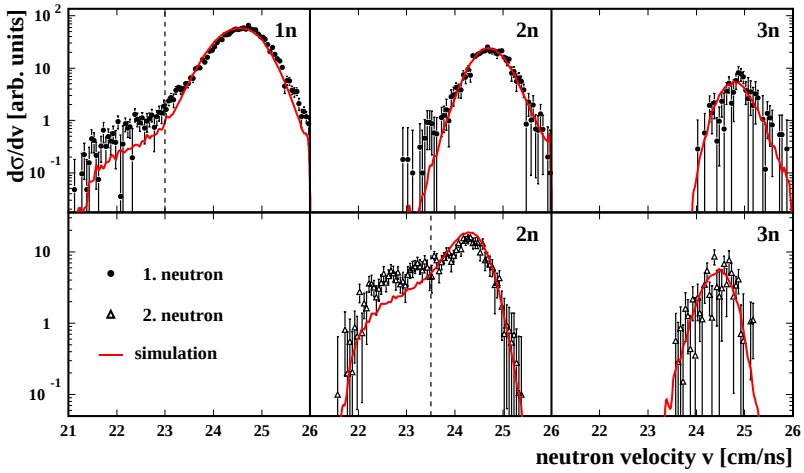

FIG. 6. (Color online) Neutron velocity spectra in the laboratory frame measured with the thick Pb target. Left-hand panel: For the one-neutron decay channel. Middle panels: For the first and second neutrons detected for the two-neutrons decay channel. Right-hand panels: for the first and second neutron detected for the three-neutron decay channel. The solid curves show the result from the Monte Carlo simulation. The dashed line indicates the cut on slow neutrons, see text.

85(30) mb for the thick Pb target and the Sn target, respectively. The counting statistics obtained with the thin Pb target was not sufficient. The value of 163(20) mb for the Pb target should be compared to the previously published DGDR cross section of 215(50) mb [4], which deviate from each other by one standard deviation. It should also be noticed that the corresponding spectrum shown in Ref. [4] was obtained after deconvoluting the measured cross section distribution with the atomic background distribution discussed above. Here, we refrain from such an attempt because deconvolution enlarges statistical fluctuations considerably.

Aside from the excitation energy spectra, our data allow to inspect carefully the different components which eventually determine the excitation energy distribution, i.e., the γ-sum energy spectra and the neutron velocity or energy spectra. The γ-sum energy spectra, which were differentiated according to the different neutron decay channels, agree very well with that obtained from our Monte Carlo simulation. The experimental neutron velocity spectra as shown in Fig. 6, however, exhibit a component of slow neutrons, which is qualitatively but not quantitatively reproduced by the calculation which assumes statistical decay. The effect appears to be most pronounced for the $2n$ channel. At high neutron velocities, slight but less pronounced deviations are also observed. Towards high velocities, however, the spectra become Lorentz compressed and deviations are more difficult to disentangle.

Attempts to remove the discrepancy by a variation of the level density parameters governing the statistical neutron decay failed. Allowing for a nonstatistical neutron decay component directly into the ground state or its near vicinity with a relative intensity of up to 10%, moreover, was also not successful. The slow neutron component, in consequence, has to be assigned either to a residual instrumental background or to a physical process that we do not control. It should be noticed that the neutron decay spectra obtained for the excitation of ^{208}Pb do not exhibit such effects, see the data presented in Sec. V B.

In order to study the influence of this unexplained neutron component, the slow neutrons were cut out, the cut being indicated in Fig. 6, and the analysis was repeated under this constraint. The excitation energy spectra obtained from this analysis are shown in Fig. 7. The cross sections for the one-phonon transitions changed only slightly, the excess cross section at high excitation energies, however, reduced to 106(17) mb in case of the thick Pb target and to 62(32) mb in case of the Sn target. The two results obtained from analyzing the data with or without cutting on the neutrons, may be considered to deliver lower and upper limits for the excess cross section. In Table II, we quote average values with sys-

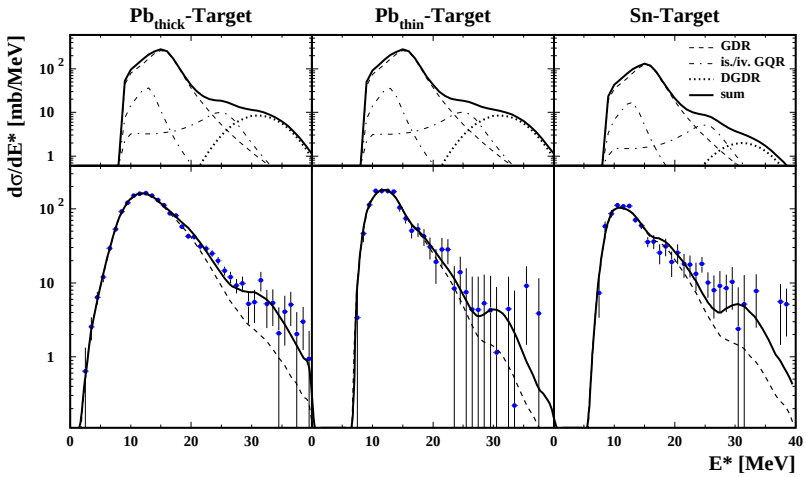

FIG. 7. (Color online) Lower panels: Experimental excitation energy spectra for ^{136}Xe (700 MeV/nucleon) on the three targets. The solid lines show the result of the data analysis including cross sections for GDR, GQR, and DGDR excitations, the dashed lines those without DGDR excitations. The calculated spectra are convoluted with the response of the detector system. Upper panels: Calculated spectra prior to convolution for the GDR, isovector and isoscalar GQR, the DGDR, and their sum, as indicated in figure.

TABLE II. Experimental results for the GDR and DGDR in ^{136}Xe in comparison to values obtained in the harmonic limit. The errors quoted for σ_{harm} result from the uncertainty in photoabsorption cross sections. For σ_{expt}(DGDR), the statistical and systematical errors are given separately, see text.

Resonance	Observable	^{136}Xe Target		
		Pb_{thick}	Pb_{thin}	Sn
GDR	σ_{expt} (mb)	1243 (14)	1380 (55)	661 (26)
GDR	σ_{harm} (mb)	1695 (250)	1695 (250)	790 (120)
DGDR	E_{expt} (MeV)	29.8(+2.5,−2.1)		
DGDR	E_{harm} (MeV)	30.6		
DGDR	Γ_{expt} (MeV)	12.2(+7.5,−3.3) (FWHM)		
DGDR	Γ_{harm} (MeV)	9.8		
DGDR	σ_{expt} (mb)	135 (20; 30)		73 (32; 15)
DGDR	σ_{harm} (mb)	90 (20)		21 (5)

tematic errors covering the results from both approaches.

In Table II, we assign the excess cross section to the excitation cross section for the double-phonon giant dipole resonance. The arguments are the following.

(i) The cross section above ≈20 MeV excitation energy cannot be attributed to a single-step excitation since the adiabatic cutoff suppresses single-step excitations dramatically, as can be verified by means of semiclassical calculations.

(ii) Since the GDR excitation is the dominant single-step process, see Fig. 7, thus the DGDR excitation should be the most likely two-step process.

We discuss in Sec. VII B possible contributions from other two-step processes.

Table II summarizes the results obtained for ^{136}Xe in comparison to the values expected within the harmonic limit for giant dipole resonance excitations. For a state formed by two non-interacting phonons, the excitation energy and the width should be twice as large as for the corresponding one-phonon state [3]. Within the experimental errors of a few MeV, no significant deviation is observed. Most noticeably, at one hand, a reduction of the single-phonon cross section, and on the other hand, an enhancement of the double-phonon cross section is observed, both in comparison to the harmonic-limit value. Averaging over all targets, the reduction of the single-phonon cross section amounts to 25(15)%, where the error is essentially reflecting the uncertainty in the photoabsorption cross sections, see Table II. A similar, somewhat larger effect was observed in the earlier measurement for ^{136}Xe [4].

V. THE RESULTS ON ^{208}Pb

Results from the ^{208}Pb experiment are partly published in Ref. [6]. Here, we briefly summarize and, in addition, provide an analysis of the giant resonance decay data delivering supplementary information.

A. The excitation energy spectra

The energy-differential cross sections for ^{208}Pb projectiles (640 MeV/nucleon) on six different targets were determined from the experiment. U (238 mg/cm^2), Pb (256 and 798 mg/cm^2), Ho (800 mg/cm^2), Sn (500 mg/cm^2), and C (180 mg/cm^2) were used as target material, all of natural abundance. The treatment of data and the analysis of the excitation spectra was performed in essentially the same manner as in the case of ^{136}Xe, for details see Ref. [6]. Figure 8 shows the excitation energy spectra for the heavier targets in comparison to the calculated cross sections.

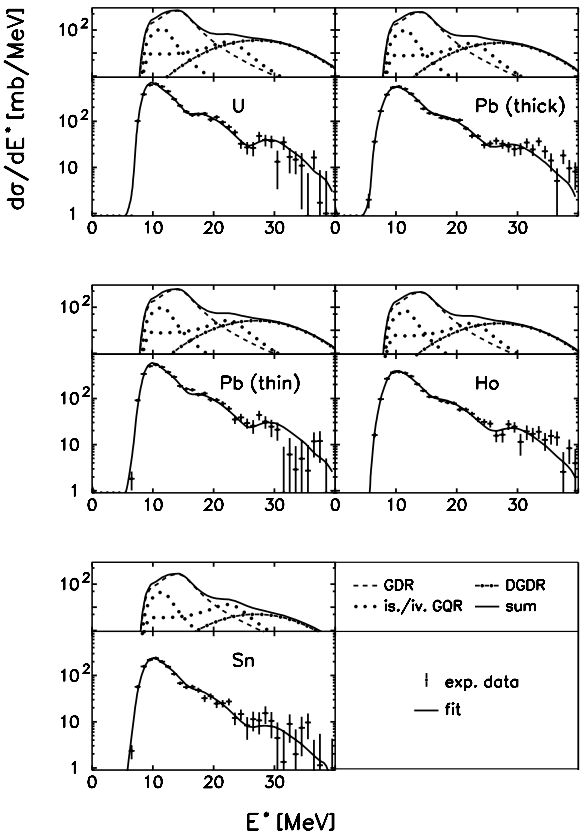

FIG. 8. Same as Fig. 7, but for ^{208}Pb (640 MeV/nucleon) on five different targets.

The giant resonance parameters entering the calculation are taken from the photoabsorption measurements [31,32] for the isovector GDR, from electron scattering data [33] for the GQR_{is}, and from Refs. [19,34] for the GQR_{iv}, see Table III. As in the case of ^{136}Xe, the cross section attributed to the DGDR was parametrized by a Gaussian distribution, parameters of which were obtained in a chi-square fitting procedure. As seen from Fig. 8, the experimental spectra can almost perfectly be reproduced by the calculated ones. Table IV summarizes the experimental data. It should be noticed

TABLE III. Same as Table I, but for ^{208}Pb.

	E_{1ph} (MeV)	Γ (MeV)	Strength (%)
GDR	13.6	3.7	110.8
	11.6	2.1	10.8
GQR_{is}	10.6	2.7	100
GQR_{iv}	22.0	5.5	100

TABLE IV. Same as Table II, but for the experimental results for ^{208}Pb.

Resonance	Observable	^{208}Pb Target				
		U	Pb_{thick}	Pb_{thin}	Ho	Sn
GDR	σ_{expt} (mb)	3595 (108)	3445 (69)	3168 (95)	2421 (48)	1427 (43)
GDR	σ_{harm} (mb)	3655	3140		2345	1515
DGDR	E_{expt} (MeV)	26.6 (8) [a]				
DGDR	E_{harm} (MeV)	26.8				
DGDR	Γ_{expt} (MeV)	6.3 (1.3) [a] (FWHM)				
DGDR	Γ_{harm} (MeV)	8.0				
DGDR	σ_{expt} (mb)	486 (90)	376 (61)	352 (65)	270 (48)	68 (30)
DGDR	σ_{harm} (mb)	378	279		158	66

[a]Average value from this experiment and that in Ref. [35].

that, in contrast to ^{136}Xe, the cross sections for the single-phonon GDR excitation agree rather well with the calculated ones based on photoabsorption measurements.

Integrated GDR and DGDR cross sections are shown in Fig. 9 as a function of the charge of the target. In a doubly logarithmical presentation, a 1.8 (3) times steeper rise of the DGDR cross section with target charge is observed as compared to that for the GDR [6]. For a two-step electromagnetic excitation in comparison to a one-step excitation, a factor of close to 2 is expected, see the semiclassical calculations shown in Fig. 9. This provides evidence that the cross section assigned to the DGDR indeed arises essentially from a two-step excitation. The lower panel of Fig. 9 compares the experimental DGDR cross section to those obtained in the harmonic limit. Averaged over all targets, we find a ratio amounting to 1.33 (16).

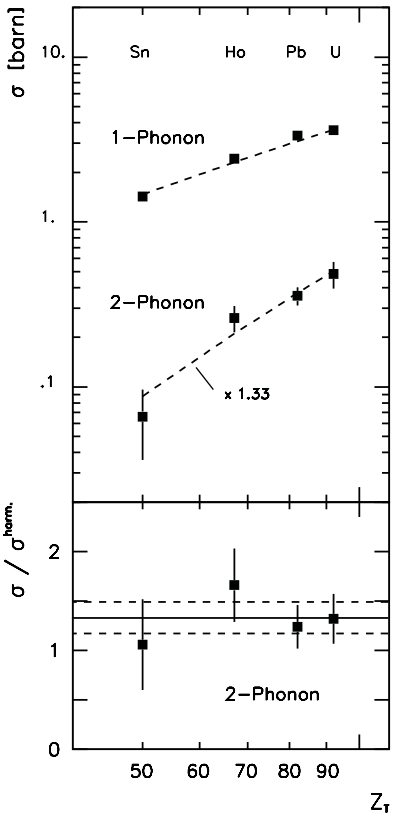

FIG. 9. Upper panel: Integrated cross sections for the GDR and the DGDR in ^{208}Pb measured on different targets of nuclear charge Z_T. The dashed lines interpolate cross-section predictions from the semiclassical calculation; in case of the DGDR, the calculated values are multiplied by a factor of 1.33. Lower panel: Ratio of the experimental cross sections for the DGDR in ^{208}Pb to the ones calculated in the harmonic limit. The mean value and its error are indicated by solid and dashed lines, respectively.

B. Decay properties

In heavy nuclei, such as ^{208}Pb, the giant resonances discussed here decay predominantly via the emission of neutrons. The Coulomb barrier suppresses decay channels involving charged particles, and the direct γ-decay back to the ground state contributes to about 1% only. Due to internal nucleon-nucleon collisions, giant resonances, manifesting a coherent superposition of one particle–one hole states, are after formation gradually transformed into complex many particle–many hole states prior to decay by particle emission. This process is reflected by the ''spreading width'' of giant resonances. These states of complex configuration most likely decay in a statistical manner. For the GDR in ^{208}Pb, two experiments [36,14] reported nonstatistical decay components contributing to less than 10% to the total decay spectrum.

In order to illuminate the decay characteristics, in particular from excitation energies around the DGDR, we inspected neutron decay spectra. For that purpose we analyzed kinetic energy (T_{kin}) spectra of the neutrons emitted from the excited projectiles after a Lorentz transformation into the projectile center-of-mass frame. In a first step, guided by the assumption of a purely statistical decay mode, we compare these spectra to a (modified) Maxwellian distribution of the form

$$d\sigma/dT_{kin} = \text{const.} T_{kin}^{n} e^{-(T_{kin}/T)} \tag{4}$$

with the slope parameter T_o being related to the excitation energy or temperature of the nucleus. In cases where only one neutron is emitted, the exponent $n=1$ is chosen, for

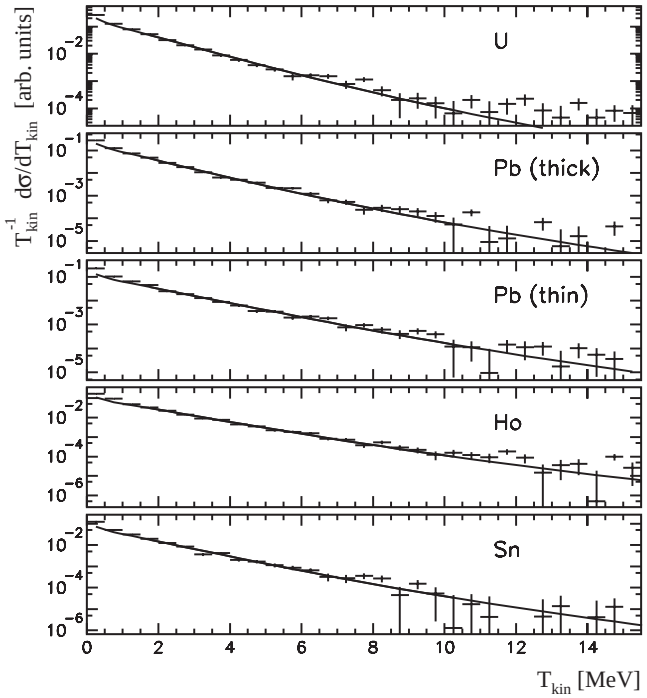

FIG. 10. Neutron kinetic energy spectra, $1/T_{kin}d\sigma/dT_{kin}$, in the ^{208}Pb projectile center-of-mass frame for different targets as indicated and for events with emission of one neutron. Solid lines represent Maxwell distributions with adjusted slope parameter T_o, see Eq. (4), after folding with the experimental response.

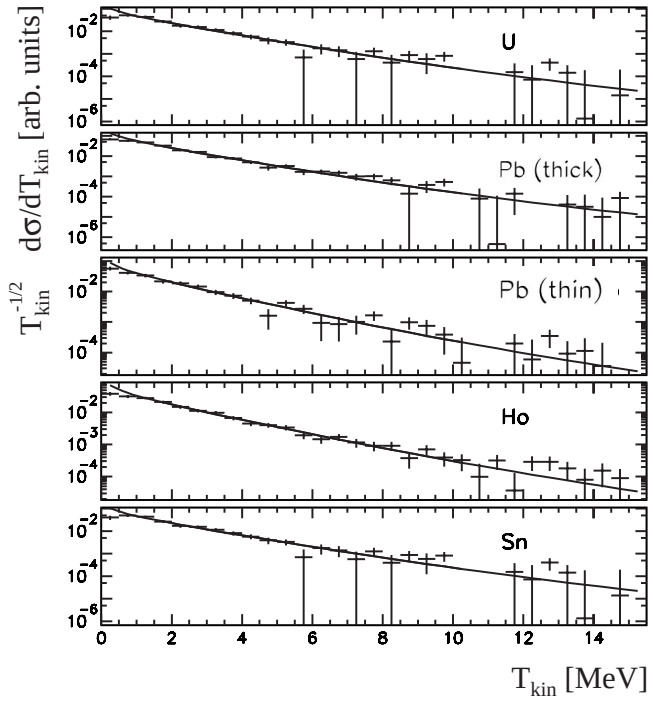

FIG. 11. Same as Fig. 10, but for events where two neutrons are emitted.

higher neutron multiplicities $n=1/2$. The latter was suggested to be appropriate in case of emission of more than one neutron [37]. Figure 10 shows the neutron kinetic energy spectra, more precisely the quantity $1/T_{kin}d\sigma/dT_{kin}$, for events of one-neutron emission; such events can be attributed solely to one-phonon excitations. The measured spectra can be well reproduced by the Maxwellian distribution over about three orders of magnitude in cross section.

Figure 11 shows the corresponding spectra, accompanied by the emission of two neutrons. Such events are more sensitive to the decay out of the DGDR domain. Again, the measured spectra appear to be well reproduced by the Maxwellian distribution.

In a second step, a more elaborated investigation of the neutron decay data was performed by comparing to calculations using the statistical decay code CASCADE [38]. Neutron decay spectra were calculated for excitation energies of $E^*=8-40$ MeV in bins of 1 MeV. The decay spectra were weighted each according to the energy differential cross sections known from the excitation energy spectra and then added up. In addition to the statistical decay, a nonstatistical neutron-decay branch was introduced accounting for a direct transition to the ground state of ^{207}Pb. The relative strength of this ''direct'' decay was a free parameter. The result is shown in Fig. 12.

The inset in this figure shows the χ^2 values per degree of freedom for different choices of relative strength of the nonstatistical component. Obviously, this component contributes to 10% at most, as was found for the GDR in Refs. [36,14].

C. Double-phonon spreading width

Combining the cross sections from this experiment on ^{208}Pb covering the GDR and DGDR neutron decay with

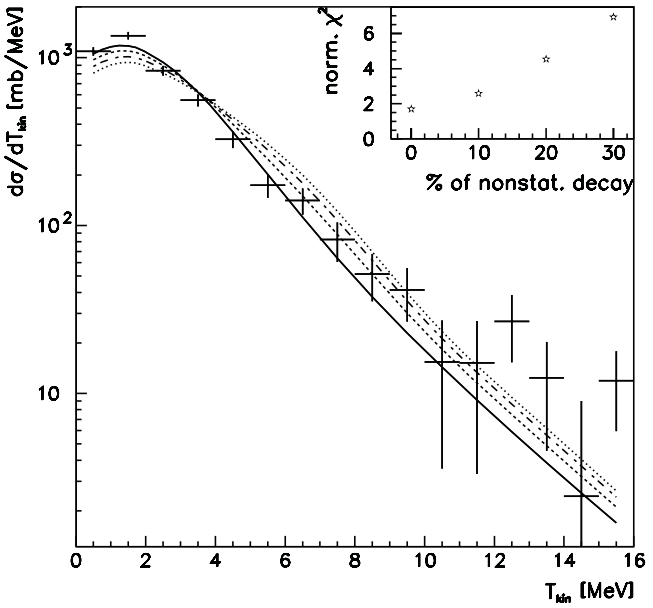

FIG. 12. Neutron kinetic energy spectra in the ^{208}Pb projectile center-of-mass frame, comprising events with emission of up to three neutrons. Calculations within the statistical model but including direct decay components (see text) contributing 0%, 10%, 20%, and 30% are shown as solid, dashed, dashed-dotted, and dotted curves, respectively. The inset shows the respective normalized χ^2 values.

those from a measurement of the direct GDR and DGDR γ-decay in the same nucleus [35], allows to determine the branching ratio $\mathrm{BR}_{\gamma/n}$ of γ and neutron decay in a straightforward manner. After scaling slightly the cross sections according to the fact that the beam energy was different for the two experiments, we deduce a one-phonon (1ph) GDR branching ratio of $BR_{\gamma/n}^{1ph}=0.019\pm0.002$ which is in good agreement with the value found in Ref. [39]. For the two-phonon (2ph) giant dipole resonance, here the branching ratio is deduced for the first time amounting to a value of $\mathrm{BR}_{2\,\gamma/n}^{2ph}=(4.5\pm1.5)\times10^{-4}$ for the double γ decay.

Using these values, one can derive the spreading width $\Gamma^{\downarrow}$ as was outlined in Ref. [3]. As shown above, the neutron decay spectra observed for ^{208}Pb do not exhibit any significant contribution from direct particle decay. Thus, the particle escape width $\Gamma^{\uparrow}$ can be ignored in the following consideration. Two processes remain competing in the destruction of the coherent giant resonance states: the direct γ back decay of width Γ_{γ} and the spreading into many particle–many hole configurations of width $\Gamma^{\downarrow}$. The branching ratios $\mathrm{BR}_{(2)\,\gamma/n}$ are thus given by the ratios $\Gamma_{\gamma}^{1ph}/(\Gamma^{\downarrow})^{1ph}$ for the one-phonon state and $\Gamma_{\gamma}^{2ph}/(\Gamma^{\downarrow})^{2ph}$ for the two-phonon state. Adopting noninteracting phonons, the $2\,\gamma$-decay branching ratio $\mathrm{BR}_{2\,\gamma/n}^{2ph}$ can be written as

$$\mathrm{BR}_{2\,\gamma/n}^{2ph}=\frac{\Gamma_{\gamma}^{2ph}}{(\Gamma^{\downarrow})^{2ph}}\,\frac{\Gamma_{\gamma}^{1ph}}{(\Gamma^{\downarrow})^{1ph}}=2\frac{(\Gamma^{\downarrow})^{1ph}}{(\Gamma^{\downarrow})^{2ph}}\left[\frac{\Gamma_{\gamma}^{1ph}}{(\Gamma^{\downarrow})^{1ph}}\right]^{2}, \quad (5)$$

therein using $\Gamma_{\gamma}^{2ph}=2\Gamma_{\gamma}^{1ph}$, i.e., the Bose factor for identical phonons. The relative spreading width $(\Gamma^{\downarrow})^{2ph}/(\Gamma^{\downarrow})^{1ph}$ may now be obtained from Eq. (5) by inserting the experimental values for the γ-decay branches. Two effects still have to be taken into account. First, as the DGDR cross section was observed to be enhanced by a factor of 1.33 ± 0.16 (see Sec. V A), Γ_{γ}^{2ph} has to be enhanced by this factor. Second, there is also a statistical component for γ transitions to the ground state contributing about 20–30 % to the total γ decay for the GDR in ^{208}Pb [39]; for the DGDR this contribution can be neglected due to the increased level density. The two effects practically cancel each other and a value of $(\Gamma^{\downarrow})^{2ph}/(\Gamma^{\downarrow})^{1ph}=1.6\pm0.5$ is determined from Eq. (5). This relative spreading width is in accordance with the ratio of apparent widths of DGDR and GDR in ^{208}Pb as quoted in Table VII amounting to $\Gamma^{2ph}/\Gamma^{1ph}=1.6\pm0.3$. Both values indicate a DGDR spreading width somewhat lower than the value $(\Gamma^{\downarrow})^{2ph}/(\Gamma^{\downarrow})^{1ph}=2$ expected for noninteracting phonons.

VI. THE RESULTS ON ^{238}U

For ^{238}U, both the neutron decay and the fission channel are open after giant resonance excitations. Here we present the results of the neutron decay analysis only. These studies are performed similarly to that of the Xe and the Pb experiment. Figure 13 shows the measured differential cross section $d\sigma/dE^{*}$ for the excitation of ^{238}U on Pb (302 mg/cm^2) and Sn (239 mg/cm^2) targets at 500 MeV/nucleon bombarding energy, as obtained for the one- to three-neutron decay channels.

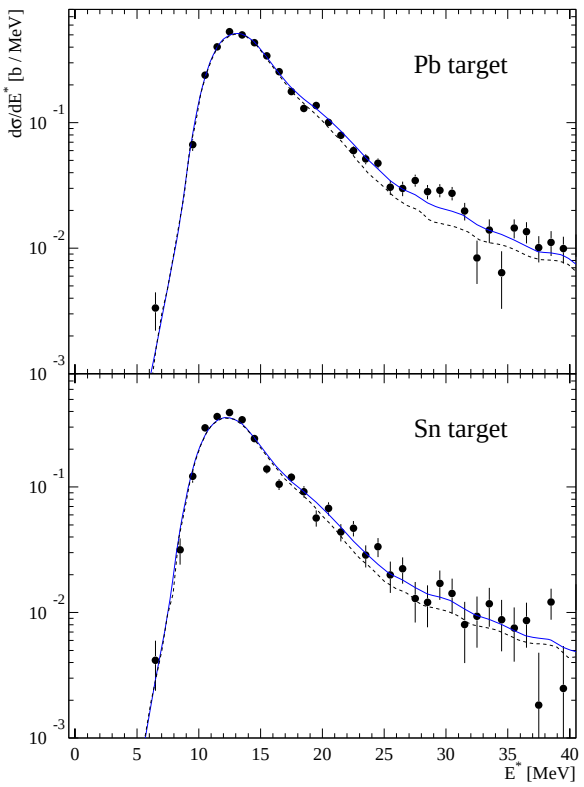

FIG. 13. (Color online) Differential cross section for the excitation and subsequent neutron decay of ^{238}U on Pb (upper panel) and on Sn (lower panel) targets at a bombarding energy of 500 MeV/nucleon. The dashed line represents cross sections calculated for one-phonon giant resonance (GDR and GQR) excitations after applying the experimental filter. The solid line reflects the sum of one-phonon and two-phonon components.

Nuclear excitation contributions were subtracted using the measurement with a carbon target (274 mg/cm^2) (compare Sec. IV B), the factor for the scaling of nuclear effects with target mass from C to Pb (Sn) target is applied according to Ref. [8], resulting in a factor of 2.0 ± 0.4 (1.8 ± 0.4).

The differential cross sections are compared to calculations as described for ^{136}Xe in Sec. IV A. The resonance parameters for the one phonon excitations are listed in Table V and were taken from photoabsorption data [40] for the GDR in ^{238}U and from electron scattering data for the $\mathrm{GQR}_{is,iv}$ [41–43]. Photoabsorption cross sections in ^{238}U exhibit a double hump structure reflecting the intrinsic quadrupole deformation of this nucleus. In the respective electro-

TABLE V. Same as Table I, but for giant resonances in ^{238}U.

	E_{1ph} (MeV)	Γ (MeV)	Strength (%)
GDR	10.77	2.37	34
	13.80	5.13	109
GQR_{is}	9.9	3.0	100
GQR_{iv}	21.6	5.0	70

TABLE VI. Ratio of cross sections for the DGDR and the GDR in ^{238}U from this experiment and from calculations in the harmonic limit.

	Pb target	Sn target
$(\sigma_{DGDR}/\sigma_{GDR})_{expt}$	0.071 (26)	0.057 (34)
$(\sigma_{DGDR}/\sigma_{GDR})_{harm}$	0.067	0.034

magnetic cross section at 500 MeV/nucleon, the upper component, however, appears to be drastically reduced due to the adiabaticity conditions in such heavy-ion collision.

The decay branchings into the various neutron and fission decay channels are known up to 18 MeV excitation energy [40] and were extrapolated for higher excitation energies following the prescription in Ref. [7].

The experimental data and the calculated energy differential cross section distributions are compared to each other in Fig. 13. Evidently, the cross section for the DGDR contributes only a very small fraction of the total observed one, since the DGDR decays to most extent into fission. Due to the low branch of the DGDR cross section into the neutron decay channels, only a restricted analysis was feasible, parameters such as width and splitting into different components expected for a strongly deformed nucleus could not be determined. Instead, as far as the DGDR is concerned, we compare the data only with the predictions obtained within the folding model. The normalizations for single-phonon and DGDR excitations, however, were varied. The calculated cross sections for the one-phonon and the DGDR excitations after passing the experimental filter and proper normalization are included in Fig. 13. The overall normalization of the experimental data, moreover, was somewhat hampered by the requirement of implementing measuring devices covering the fission channel as well, see Sec. III C. We thus prefer to quote only the ratio of the GDR and DGDR cross section where uncertainties in normalization cancel. The result is given in Table VI. Within errors, this ratio is found to be in agreement with that of the harmonic prediction and confirms the earlier result from an inclusive measurement of the neutron decay in Ref. [7].

VII. SUMMARY OF EXPERIMENTAL RESULTS AND DISCUSSION

A. Summary

The results from the experiments for ^{136}Xe, ^{208}Pb, and ^{238}U may be summarized as follows

(1) Peripheral collisions between two heavy ions at bombarding energies of several hundreds of MeV/nucleon give rise to inelastic excitations in the domain of up to several tens of MeV in excitation energy with cross sections of the order of several barns. These cross sections are essentially due to electromagnetic excitation processes.

(2) The measurement of the angular distribution of the scattered projectile in case of ^{136}Xe appears to be well reproduced within the framework of the semiclassical approach. A minimum impact parameter separates rather sharply the domain of electromagnetic excitations from that of nuclear processes resulting in absorption.

(3) The ^{208}Pb measurement with five different targets, at one hand, shows that the overwhelming part of the cross section can be understood as an electromagnetic single-step excitation to the giant dipole resonance with small contributions from quadrupole resonances. On the other hand, the excess cross section observed at excitation energies above the one-phonon resonances was found to arise essentially from a two-step excitation mechanism, thus is most likely to be assigned to the double-phonon giant dipole resonance. The parameters deduced for the DGDR are, at least qualitatively, in accord with the expectations within the harmonic limit. Yet, depending on the nucleus, an enhancement in excitation cross section for the DGDR is observed if compared to the folding model based on a harmonic response.

(4) The neutron decay seems to be governed by statistical decay properties. Only for ^{136}Xe, a small deviating component was observed, the origin of which is not clear. In ^{208}Pb, both the DGDR apparent width and the DGDR spreading width extracted independently from our data together with that for the double-γ decay indicate a value somewhat lower than expected for noninteracting phonons.

TABLE VII. Double-phonon giant dipole parameters, i.e., peak energy E, apparent width Γ, and cross section σ (σ^{cor}) from this experiment in relation to their values adopting a harmonic dipole response. σ and σ^{cor} denote cross sections prior to and after corrections for contributions from GDR$\otimes$GQR excitations, respectively. The value given in square brackets for ^{208}Pb is that for the spreading width. The data available from different targets were averaged. The second error quoted for σ/σ_{harm} for ^{136}Xe represents the systematic error, see text.

DGDR	E/E_{harm}	Γ/Γ_{harm}	σ/σ_{harm}	$\sigma^{cor}/\sigma_{harm}$
^{136}Xe	0.97 (8)	$1.25(^{+77}_{-34})$	1.54 (22; 30)	1.35 (21; 26)
^{208}Pb	0.99 (3)	0.79 (16) [0.80 (25)]	1.33 (16)	1.08 (13)
^{238}U			1.13 (36)	0.90 (29)

Table VII summarizes the DGDR results from the experiments reported here by comparing to the values obtained adopting a harmonic response. The values quoted are those obtained after averaging the results from different targets.

B. Discussion

Experimental studies of double-phonon giant resonances stimulated a considerable theoretical activity, essentially at two frontiers: microscopic calculations for the double-phonon nuclear response and reaction dynamics studies, the latter ones to most extent concerned with the apparent enhancement of the electromagnetic DGDR cross sections. For a comprehensive overview of the various efforts we refer to

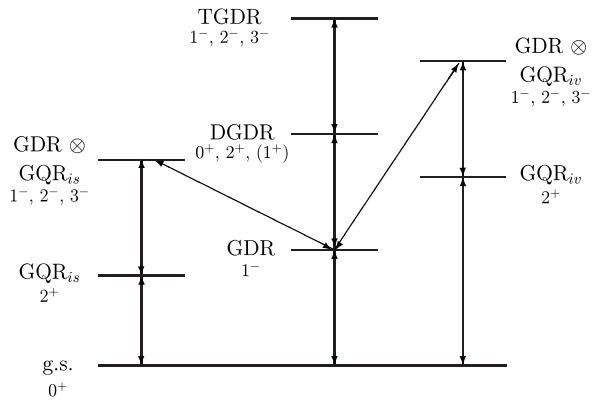

FIG. 14. Excitation pathways adopted for the coupled-channels calculation estimating cross sections for two-phonon states of type GDR⊗GQR. TGDR denotes three-phonon giant dipole resonances.

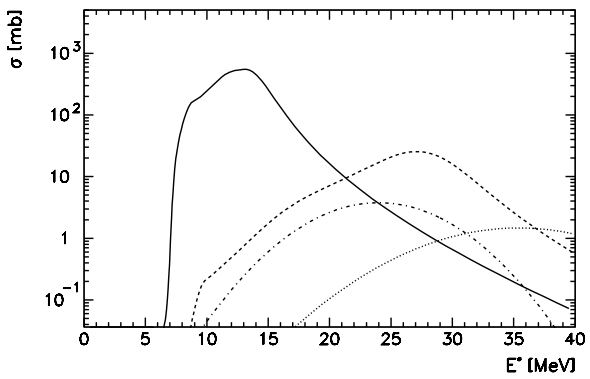

FIG. 15. Cross section distributions for the GDR (solid line) and double-phonon states populated in ^{208}Pb projectiles (640 MeV/nucleon) impinging on a Pb target: DGDR (dashed line), GDR $\otimes$GQR$_{is}$ (dashed-dotted line), GDR$\otimes$GQR$_{iv}$ (dotted line).

the most recent review papers [3,44] and the references given therein. Here, we restrict ourselves to the most extensively discussed topics: (i) a physical background in the DGDR excitation energy regime from two-phonon states of other character than the DGDR, (ii) the role of an anharmonic nuclear response, and (iii) effects due to damping of the coherent one-phonon state during the heavy-ion collision.

Contributions from other two-phonon states. So far, the cross section observed on top of that from one-phonon giant resonance was assigned to the DGDR solely. It was discussed in Refs. [45–47] that other two-phonon states may contribute to the experimentally observed cross sections. There, for the specific case of ^{208}Pb, it was derived on the basis of microscopic calculations that the excitation of such states could increase the cross section in the DGDR energy regime on a level of about 20%, thus reproducing almost quantitatively the measured cross section. The most significant contribution stems from two-phonon states built by coupling of a GDR phonon with a GQR phonon.

In order to illuminate the magnitude of such contributions, we performed coupled-channels calculations for the nuclei under investigation. The adopted scheme of excitation pathways is shown in Fig. 14. The required excitation energies and transition matrix elements for the single-phonon excitations were extracted from experimental quantities, see Tables I, III, and V. The transition matrix elements for the multiphonon states were deduced from that between ground state and one-phonon state applying the relevant spin factors and, in case of identical phonons, the Bose factors.

The coupled-channels calculations result in a cross section of 15–20 % in case of GQR$_{is}\otimes$GDR and to about 10% in case of GQR$_{iv}\otimes$GDR, relative to that of the DGDR. For ^{208}Pb, these values are of similar magnitude as found in the RPA calculations in Ref. [45]. The coupled-channels calculations are schematic to the extent that the width of the giant resonances is ignored. In order to illustrate the overlap of the various two-phonon states, we convoluted the calculated cross section with the respective width of the two one-phonon states involved, the result is shown for ^{208}Pb in Fig. 15. It appears that the GQR$_{is}\otimes$GDR state fully overlaps and the GQR$_{iv}\otimes$GDR overlaps to about 50% with the DGDR. Tentatively, we subtracted these contributions, resulting in corrected DGDR cross sections which are included in Table VII and, for the Pb target, are shown in Fig. 16.

Anharmonicities. Naturally, the investigation of the DGDR spectral distribution is concerned with the question to which extent a harmonic behavior is obeyed.

To which extent anharmonicities effect the electromagnetic DGDR cross sections was studied in a more empirical approach in Refs. [48–50]. Therein, an anharmonic vibration was considered with parameters governing the degree of anharmonicity being introduced ad hoc. The results of Ref. [48], in particular, inferred that even modest anharmonicities can affect the DGDR cross sections considerably. In Ref. [50], a similar type of calculation was performed; DGDR energy shifts were combined with a change of the oscillator frequency in order to assure that the energy of the single GDR remains at its experimentally known value. This calculation resulted in much smaller effects on DGDR cross sections in comparison to those of [48].

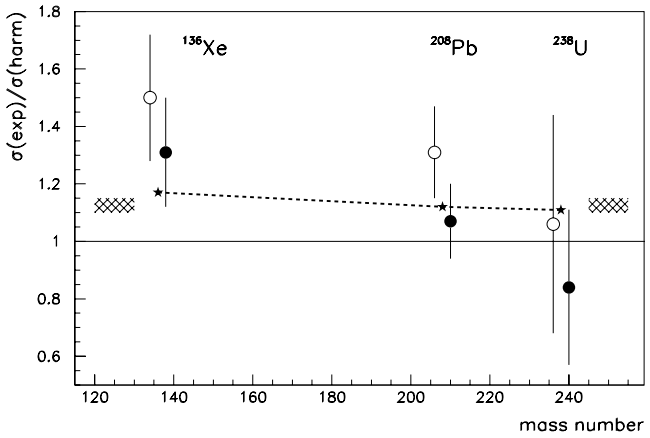

FIG. 16. Experimental DGDR cross sections relative to their harmonic values prior to (open circles) and after (filled circles) subtraction of contributions from two-phonon states of type GDR $\otimes$GQR for the three measured nuclei on a Pb target. The hatched areas indicate the expected increase of the cross sections due phonon damping during the collision. Star symbols (connected by a dashed line) reflect the increase of cross section due to an anharmonic dipole response relative to the harmonic response (see text).

In a number of microscopic calculations, energy shifts and the splitting of the DGDR resonance into its $I^{\pi}=0^{+}$ and 2^{+} spin components were derived, see Refs. [3,44] for a survey. Such studies, in general, result in small relative energy shifts of the order of typically a few hundreds of keV in heavier nuclei, with mass dependencies proportional to A^{-1} [51] or $A^{-4/3}$ [52,53], see also Ref. [54]. The systematic calculations of Ponomarev *et al.* [51] spanning over a wide range in mass yielded, for example, an energy shift of the DGDR 2^{+} state in ^{208}Pb of -158 keV and a mass (A) dependence of the DGDR energy shift was found of the form $\Delta E=bA^{-\alpha}$ with $b=-37(8)$ MeV and $\alpha=1.08(6)$. One- and two-phonon configurations were included in this calculation. In Ref. [55], selected three-phonon configurations were included which appeared to have a minor effect on the DGDR energy shift.

Very recently, however, it was shown by Fallot *et al.* [56] that the inclusion of specific three-phonon states can be crucial. The DGDR, in particular, seems to be influenced most strongly by its mixing with a three-phonon state built from two dipole and one monopole giant resonance phonon. According to Ref. [56], the coupling of two-phonon states with three-phonon states yields considerably larger down-shifts of the two-phonon spectrum. For example, the DGDR 2^{+} state was found to be shifted by -600 keV, i.e., four times the value obtained in Ref. [51].

Unfortunately, such energy shifts of below about 1 MeV cannot be resolved with the present experimental techniques. A shift of E_{DGDR}, however, influences the electromagnetic excitation strength in a twofold way, first due to the adiabatic cutoff of the virtual phonon spectrum and second, due to the related change in the transition matrix element. Both effects enhance (decrease) the cross section for lower (higher) values of E_{DGDR} in comparison to the harmonic limit.

In order to illustrate the effect of an anharmonicity on the electromagnetic excitation cross sections, we performed coupled-channel calculations for the nuclei under investigation. For that purpose, we adopted the result of Fallot *et al.* for the case of ^{208}Pb, which we scale according to an A^{-1} dependence in order to obtain values for ^{136}Xe and ^{238}U, i.e., for the DGDR 2^{+} state we adopt an energy shift $\Delta E=-125A^{-1}$ MeV. The relevant $E1$ matrix elements were then computed using Eqs. (8)–(11) provided in Ref. [50] for an anharmonic oscillator. The results of our calculation are shown in Fig. 16 and should be compared to the experimental data after subtraction of the GDR$\otimes$GQR contributions (filled circles in Fig. 16). The DGDR cross sections increase by about 10–20 % and approach the experimental data more closely. The calculations, however, should be considered as only schematic ones, a more correct treatment would require to deduce energy shifts and splittings as well as transition matrix elements from a microscopic approach in a consistent manner, an approach beyond the scope of this experimental paper.

Dynamical effects. Dynamical effects due to the spreading width of the giant dipole resonance were discussed in the literature [57–62]. The basic idea is that, during the collision, the excited coherent one-phonon state according to its spreading width is transformed into a state of ''complex'' many particle–many hole states. This process, in principle, depletes the flux available for forming a coherent two-phonon state during the ongoing electromagnetic interaction in the heavy-ion collision, see, e.g., Ref. [61]. It was pointed out in Ref. [60], however, that a GDR phonon may be built on top of the complex state as well according to the Brink-Axel hypothesis. A second excitation pathway thus opens up which may add to the coherent two-phonon excitation and which could modify the DGDR cross section. Very recently, this idea was followed up by Gu and Weidenmüller [62] who performed detailed calculations applying random-matrix theory. For the system ^{208}Pb (640 MeV/nucleon) on a Pb target as investigated experimentally here, both calculations [60,62] find an increase of the DGDR cross section.

The magnitude of the effect is governed by the time scale on which the spreading proceeds, $\tau_d \approx \hbar/\Gamma^{\downarrow}$, in proportion to the time interval during which the Coulomb interaction induces phonon excitations, $\tau_c \approx 2b/\gamma v$, depending on impact parameter b and the projectile velocity v. To illustrate, we quote the ratio τ_c/τ_d for the collisional systems under investigation for an impact parameter of 15 fm, around which the cross section for two-phonon excitation peaks; values of $\tau_c/\tau_d=0.52$, 0.41, and 0.58 for ^{136}Xe, ^{208}Pb, and ^{238}U are obtained, respectively. These values vary only little for the collision systems investigated here, and the effect on the DGDR cross sections should be very similar in magnitude, in case of ^{136}Xe and ^{238}U slightly higher than in case of ^{208}Pb. For the latter case, i.e., ^{208}Pb (640 MeV/nucleon) on a Pb target, a DGDR cross section enhancement of 10% was obtained from the calculations of Ref. [62], see R_2 values in Fig. 3 therein, and 14% from that of Ref. [60], see Fig. 7 therein. It may thus be guessed that the effect of damping of the coherent phonon state during the collision should increase the DGDR cross sections by 10–15 % for all three systems investigated here. This enhancement of DGDR cross section is indicated in Fig. 16.

We notice that the calculations in Ref. [60] also predict a reduction in cross section for the single-phonon GDR, too small, however, in comparison to the reduction observed here for ^{136}Xe. In order to investigate systematically the effect of the spreading width, experiments would have to be performed at much lower bombarding energies, typically 100 MeV/nucleon, at which the increase of cross section is predicted to be much more pronounced.

VIII. CONCLUSION

Single- and double-phonon states of the isovector giant dipole resonance were observed in high-energy heavy-ion collisions with cross sections amounting to several barns and several hundreds of millibarns, respectively. Cross section distributions with regard to scattering angle and excitation energy are quantitatively described by electromagnetic excitation treated in semiclassical approximation. Integrated one-phonon cross sections are in accord with photoabsorption measurements, only for ^{136}Xe a significant reduction was found which may be linked to observed small nonstatistical neutron-decay components.

The neutron decay out of the DGDR excitation energy domain was studied in detail for ^{208}Pb and, here, exhibits

essentially statistical features only. From a combination of results of the neutron decay measurement presented here and an earlier two-photon decay experiment, the spreading width of the DGDR in ^{208}Pb could be obtained.

The integrated cross sections in the domain of the double-phonon giant dipole resonance appear, depending on the nucleus, to be enhanced in comparison to the cross section expected relying on a harmonic dipole response. A number of effects were discussed, each of which increases the DGDR cross section on a level of 10–20 %, and the cumulative action of which may eventually be responsible for the observed cross section enhancement: Contributions from the excitation of two-phonon states of type GDR$\otimes$GQR; the spreading of the one-phonon state during the heavy-ion collision; an anharmonic dipole response. At present, the individual contributions from such effects cannot be disentangled on experimental grounds and remain a challenging task for measurements with advanced methods.

ACKNOWLEDGMENTS

We thank P. F. Bortignon, V. Yu. Ponomarev, and W. Nörenberg for many fruitful discussions. This work was supported by the German Federal Minister for Education and Research (BMBF) under Contract Nos. 06 OF 933 and 06 MZ 963 and by GSI via Hochschulzusammenarbeitsvereinbarungen under contracts OF ELZK, MZ KRAK, and by the Polish Committee of Scientific Research under Contract No. PB2/P03B/113/09.

[1] S. Mordechai, H. Fortune, J. O'Donell, G. Lui, M. Burlein, A. Waosmaa, S. Greene, C. Morris, N. Auerbach, S. Yoo, and C. Moore, Phys. Rev. C **41**, 202 (1990).
[2] P. Chomaz and N. Frascaria, Phys. Rep. **252**, 275 (1995).
[3] T. Aumann, P.F. Bortignon, and H. Emling, Annu. Rev. Nucl. Part. Sci. **48**, 351 (1998).
[4] R. Schmidt, T. Blaich, Th.W. Elze, H. Emling, H. Freiesleben, K. Grimm, W. Henning, R. Holzmann, J.G. Keller, H. Klingler, R. Kulessa, J.V. Kratz, D. Lambrecht, J.S. Lange, Y. Leifels, E. Lubkiewicz, E. Moore, E. Wajda, W. Prokopowicz, C. Schütter, H. Spies, K. Stelzer, J. Stroth, W. Walús, H.J. Wollersheim, M. Zinser, and E. Zude, Phys. Rev. Lett. **70**, 1767 (1993).
[5] A. Grünschloß, K. Boretzky, T. Aumann, C. Bertulani, J. Cub, W. Dostal, B. Eberlein, Th.W. Elze, H. Emling, J. Holeczek, R. Holzmann, M. Kaspar, J.V. Kratz, R. Kulessa, Y. Leifels, A. Leistenschneider, E. Lubkiewicz, S. Mordechai, I. Peter, P. Reiter, M. Rejmund, H. Simon, K. Stelzer, A. Surowiec, K. Sümmerer, J. Stroth, E. Wajda, W. Walus, S. Wan, and H. Wollersheim, Phys. Rev. C **60**, 051601 (1999).
[6] K. Boretzky, J. Stroth, E. Wajda, T. Aumann, T. Blaich, J. Cub, Th.W. Elze, H. Emling, W. Henning, R. Holzmann, H. Klingler, R. Kulessa, J.V. Kratz, D. Lambrecht, Y. Leifels, E. Lubkiewicz, K. Stelzer, W. Walus, M. Zinser, and E. Zude, Phys. Lett. B **384**, 30 (1996).
[7] T. Aumann, K. Sümmerer, H. Geissel, B. Blank, T. Brohm, H.-G. Clerc, S. Czajkowski, C. Donzaud, A. Grewe, E. Hanelt, A. Heinz, H. Irnich, A.J.M. de Jong, J.V. Kratz, A. Magel, G. Münzenberg, F. Nickel, M. Pfützner, A. Piechaczek, C. Röhl, C. Scheidenberger, K.-H. Schmidt, W. Schwab, S. Steinhäuser, W. Trinder, and B. Voss, Z. Phys. A **352**, 163 (1995).
[8] T. Rubehn, W. Müller, R. Bassini, M. Begemann-Blaich, T. Blaich, A. Ferrero, C. Gross, G. Imme, I. Iori, G. Kunde, W. Kunze, V. Lindenstruth, U. Lynen, T. Möhlenkamp, L. Moretto, B. Ocker, J. Pochodzalla, G. Raciti, S. Reito, H. Sann, A. Schüttauf, W. Seidel, V. Serfling, W. Trautmann, A. Trzcinski, G. Verde, A. Wörner, E. Zude, and B. Zwieglinski, Z. Phys. A **353**, 197 (1995).
[9] P. Armbruster, M. Bernas, S. Czajkowski, H. Geissel, T. Aumann, P. Dessagne, C. Donzaud, E. Hanelt, A. Heinz, M. Hesse, C. Kozhuharov, C. Miehe, G. Münzenberg, M. Pfützner, K.-H. Schmidt, W. Schwab, C. Stéphan, K. Sümmerer, L. Tassan-Got, and B. Voss, Z. Phys. A **355**, 191 (1996).
[10] K.-H. Schmidt, S. Steinhäuser, C. Böckstiegel, A. Grewe, A. Heinz, A.R. Junghans, J. Benlliure, H.G. Clerc, M. de Jong, J. Müller, M. Pfützner, and B. Voss, Nucl. Phys. **A665**, 221 (2000).
[11] J. Cub, G. Stengel, A. Grünschloß, K. Boretzky, T. Aumann, W. Dostal, B. Eberlein, Th.W. Elze, H. Emling, G. Ickert, J. Holeczek, R. Holzmann, J.V. Kratz, R. Kulessa, Y. Leifels, H. Simon, K. Stelzer, J. Stroth, A. Surowiec, and E. Wajda, Nucl. Instrum. Methods Phys. Res. A **402**, 67 (1998).
[12] T. Blaich, Th.W. Elze, H. Emling, H. Freiesleben, K. Grimm, W. Henning, R. Holzmann, G. Ickert, J.G. Keller, H. Klingler, W. Kneissl, R. König, R. Kulessa, J.V. Kratz, D. Lambrecht, J.S. Lange, Y. Leifels, E. Lubkiewicz, M. Proft, W. Prokopowicz, C. Schütter, R. Schmidt, H. Spies, K. Stelzer, J. Stroth, W. Walús, E. Wajda, H.J. Wollersheim, M. Zinser, and E. Zude, Nucl. Instrum. Methods Phys. Res. A **314**, 136 (1992).
[13] S. Wan, J. Gerl, J. Cub, J. Holeczek, P. Reiter, D. Schwalm, T. Aumann, K. Boretzky, W. Dostal, B. Eberlein, H. Emling, C. Ender, Th.W. Elze, H. Geissel, A. Grünschloß, R. Holzmann, N. Iwasa, M. Kaspar, A. Kleinböhl, O. Koschorrek, Y. Leifels, A. Leistenschneider, I. Peter, H. Schaffner, C. Scheidenberger, R. Schubert, H. Simon, G. Stengel, A. Surowiec, and H. Wollersheim, Eur. Phys. J. A **6**, 167 (1999).
[14] D. Chmielewska, A.M. van den Berg, Y. Blumenfeld, N. Alamanos, F. Auger, J. Blomgren, J. Bordewijk, S. Brandenburg, N. Frascaria, A. Gillibert, L. Nilsson, N. Olsson, P. Roussel-Chomaz, J.C. Roynette, J.A. Scarpaci, T. Suomijarvi, R. Turcotte, and A. van der Woude, Nucl. Phys. **A569**, 383c (1994).
[15] A. Winther and K. Alder, Nucl. Phys. **A319**, 518 (1979).
[16] S.S. Dietrich and B.L. Berman, At. Data Nucl. Data Tables **38**, 199 (1988).
[17] R. Pitthan, H. Hass, D. Meyer, F. Buskirk, and J. Dyer, Phys. Rev. C **19**, 1251 (1979).
[18] F. Bertrand, Nucl. Phys. **A354**, 129c (1981).
[19] A. van der Woude, Int. Rev. Nucl. Phys. **7**, 100 (1991).
[20] W.J. Llope and P. Braun-Munzinger, Phys. Rev. C **41**, 2644 (1990).

[21] C.J. Benesh, B.C. Cook, and J.P. Vary, Phys. Rev. C **40**, 1198 (1989).
[22] S. Kox, A. Gamp, C. Perrin, J. Arvieux, R. Bertholet, J. Bruandet, M. Buenerd, R. Cherkaoni, A. Cole, Y. El-Masri, N. Longequene, J. Menet, F. Merchez, and J. Viano, Phys. Rev. C **35**, 1678 (1987).
[23] T. Aumann, C. Bertulani, and K. Sümmerer, Phys. Rev. C **51**, 416 (1995).
[24] T. Aumann, K. Sümmerer, E. Stiel, J.V. Kratz, W. Brüchle, M. Schädel, G. Wirth, M. Fauerbach, and J. Hill, Phys. Rev. C **47**, 1728 (1993).
[25] M. Mercier, J. Hill, F. Wohn, C. McCullough, M. Nieland, J. Winger, C. Howard, S. Renwick, D. Matheis, and A. Smith, Phys. Rev. C **33**, 1655 (1986).
[26] J.C. Hill, F. Wohn, J. Winger, M. Khayat, K. Leininger, and A. Smith, Phys. Rev. C **38**, 1722 (1988).
[27] J. Hill, F. Wohn, D. Schwellenbach, and A. Smith, Phys. Rev. B **273**, 371 (1991).
[28] K. Boretzky, Ph.D. thesis, University Frankfurt, Germany, 1995.
[29] E. Erba, U. Facchini, and E.S. Menichella, Nuovo Cimento **XXII**, 1237 (1961).
[30] W. Dilg, W. Schantl, and H. Vonach, Nucl. Phys. **A217**, 269 (1973).
[31] A. Vessiére, H. Beil, R. Bergere, P. Carlos, and A. Lepretre, Nucl. Phys. **A159**, 561 (1970).
[32] K.P. Schelhaas, J.M. Henneberg, M. Sanzone-Arenhövel, N. Wieloch-Laufenberg, U. Zurmühl, and B. Ziegler, Nucl. Phys. **A489**, 189 (1988).
[33] F.E. Bertrand, Annu. Rev. Nucl. Part. Sci. **26**, 457 (1976).
[34] D.S. Dale, R.M. Laszewski, and R. Alarcon, Phys. Rev. Lett. **68**, 3507 (1992).
[35] J. Ritman, F.-O. Berg, W. Kühn, V. Metag, R. Novotny, M. Notheisen, P. Paul, M. Pfeiffer, O. Schwalb, H. Löhner, L. Venema, A. Gobbi, N. Herrmann, K. Hildenbrand, J. Mösner, R. Simon, K. Teh, J. Wessels, and T. Wienold, Phys. Rev. Lett. **70**, 533 (1993).
[36] R. Alarcon, P.L. Cole, D.S. Dale, P.T. Debevec, and L.J. Morford, Phys. Rev. C **43**, R2470 (1991).
[37] K. LeCouteur and D. Lang, Nucl. Phys. **19**, 32 (1959).
[38] F. Pühlhofer, Nucl. Phys. **A280**, 267 (1977).
[39] J.R. Beene, F.E. Bertrand, D.J. Horen, R.L. Auble, B.L. Burks, J.G. del Campo, M.L. Halbert, R.O. Sayer, W. Mittig, Y. Schutz, J. Barette, N. Alamanos, F. Auger, B. Fernandez, A. Gillibert, B. Haas, and J.P. Vivien, Phys. Rev. C **41**, 920 (1990).
[40] J.T. Caldwell, E.J. Dowdy, B.L. Berman, R.A. Alvarez, and P. Meyer, Phys. Rev. C **21**, 1215 (1980).
[41] R. Pitthan, F. Buskirk, W. Houk, and R. Moore, Phys. Rev. C **21**, 28 (1980).
[42] T. Weber, R. Heil, U. Kneissl, W. Wilke, T. Kihm, K. Knöpfle, and H. Emrich, Nucl. Phys. **A510**, 1 (1990).
[43] F. Gerab and M. Martins, Phys. Rev. C **48**, 105 (1993).
[44] C.A. Bertulani and V.Yu. Ponomarev, Phys. Rep. **321**, 139 (1999).
[45] E.G. Lanza, M.V. Andrés, F. Catara, P. Chomaz, and C. Volpe, Nucl. Phys. **A636**, 452 (1998).
[46] E.G. Lanza, M.V. Andrés, F. Catara, P. Chomaz, and C. Volpe, Nucl. Phys. **A654**, 792c (1999).
[47] E.G. Lanza, Nucl. Phys. **A687**, 162c (2001).
[48] P.F. Bortignon and C.H. Dasso, Phys. Rev. C **56**, 574 (1997).
[49] C. Volpe, F. Catara, P. Chomaz, M.V. Andres, and E.G. Lanza, Nucl. Phys. **A589**, 521 (1995).
[50] D.T. de Paula, T. Aumann, L.F. Canto, B.V. Carlson, H. Emling, and M.S. Hussein, Phys. Rev. C **64**, 064605 (2001).
[51] V.Yu. Ponomarev, P.F. Bortignon, R.A. Broglia, and V.V. Voronov, Phys. Rev. Lett. **85**, 1400 (2000).
[52] G.F. Bertsch and H. Feldmeier, Phys. Rev. C **56**, 839 (1997).
[53] I. Hamamoto, Phys. Rev. C **60**, 054320 (1999).
[54] G.F. Bertsch, P.F. Bortignon, and K. Hagino, Nucl. Phys. **A657**, 59 (1999).
[55] V.Yu. Ponomarev, P.F. Bortignon, R.A. Broglia, and V.V. Voronov, Z. Phys. A **356**, 251 (1996).
[56] M. Fallot, Ph. Chomaz, M. V. Andres, F. Catara, E. G. Lanza, and J. A. Scarpaci, Nucl. Phys. (submitted).
[57] S. Typel and G. Baur, Phys. Rev. C **49**, 379 (1994).
[58] C.A. Bertulani and V. Zelevinsky, Nucl. Phys. **A568**, 931 (1994).
[59] L.F. Canto, A. Romanelli, M.S. Hussein, and A.F.R. de Toledo Piza, Phys. Rev. Lett. **72**, 2147 (1994).
[60] B.V. Carlson, M.S. Hussein, A.F.R. de Toledo Piza, and L.F. Canto, Phys. Rev. C **60**, 014604 (1999).
[61] G. Baur, C.A. Bertulani, and D. Dolci, Eur. Phys. J. A **7**, 55 (2000).
[62] J.Z. Gu and H.A. Weidenmüller, Nucl. Phys. **A690**, 382 (2001).